Electronic Supplementary Information

Prebiotic RNA polymerisation: Energetics of nucleotide adsorption and polymerisation on clay mineral surfaces

S. Jelavić[a†], D. J. Tobler[a], T. Hassenkam[a], J. J. DeYoreo [b,c], S.L.S. Stipp[a] and K.K. Sand[a,b,d]

[a] Nano-Science Center, Department of Chemistry, University of Copenhagen, Universitetsparken 5, Copenhagen 2100, Denmark

[b] Physical Sciences Division, Pacific Northwest National Laboratory, Richland, WA, USA 99352

[c] Department of Materials Science and Engineering, University of Washington, Seattle, WA, USA 98195

[d] Currently at: a) and Geography & Earth Sciences, Aberystwyth University, UK

[†]Corresponding author: stanislav.jelavic@nano.ku.dk

Experimental details:

1. X-ray photoelectron spectroscopy (XPS)

We used XPS to assess the extent of adventitious organic carbon on our mineral substrates and for controlling the quality and the thickness of the self-assembled monolayers (SAM) on the AFM tips. Experiments were performed with a Kratos AXIS Ultra[DLD] instrument using a monochromatic AlKα radiation and a charge neutralising system. Analyser pass energy for wide spectra was 160 eV and for high-resolution spectra, it was 20 eV. Data were analysed with the CasaXPS software with the associated relative sensitivity factors that were used for quantitative analysis.

2. Cleaning and characterisation of the substrates used as models for clay mineral surfaces

Experiments were carried out on three substrates: a polished {0001} surface of a natural specular hematite, a polished {0001} surface of synthetic corundum (MTI Corp.) and a freshly cleaved {0001} surface of muscovite mica (Ted Paella, Inc.). Substrates were cleaned before every measurement to remove particulate and organic contamination from mineral surfaces. The hematite crystal was kept in 1 M NaOH solution at 60 °C for 1 hour, sonicated for 20 min to remove particulate contaminants and cleaned for 30 min in an UV/ozone chamber to decrease the amount of adventitious organic carbon compounds (unavoidable organic contamination adsorbed from the air or solution). Corundum was cleaned following

the procedure of Argyris et al.[1]; briefly, the crystal was sonicated in acetone for 20 min, dried with N_2 and treated in an UV/ozone chamber for 30 min. The same steps were then repeated, using ethanol as the solvent and treatment in the UV/ozone chamber for 40 min. All chemicals were of analytical grade (Sigma-Aldrich). Mica was cleaved immediately prior to the analysis with a piece of tape; no additional cleaning steps were made. We determined the amount of adventitious carbon on the cleaned surfaces using XPS. Surface carbon on the cleaned hematite was 6.9 ± 0.7 at.%, on cleaned corundum was 4.0 ± 0.5 at.% and on mica after cleaving was 4.5 ± 0.1 at.%. Values represent the average of three analyses (± the range) collected on three spots on the same specimen.

3. Functionalisation of atomic force microscopy (AFM) tips for the dynamic force spectroscopy (DFS) measurements and the purity and thickness of the SAMs

We used MSCT (Bruker) in house Au coated tips for DFS measurements. The spring constants of cantilevers were calculated using a thermal calibration method.[2] The tips were cleaned in the UV/ozone chamber for at least 10 min and placed in 1 mM ethanol solution of 11-mercaptoundecylphosphoric acid ($HS\text{-}(CH_2)_{11}H_2PO_4$, 90%; Sigma-Aldrich) for preparation of the phosphate tips or 1.3 mM diethyl ether of 4-(12-mercaptododecyl)pyridine ($HS\text{-}(CH_2)_{12}C_5H_5N$)[3] for preparation of pyridine tips. Tips were left in the functionalising solutions for a minimum of 18 hours to form self assembled monolayers (SAM) with phosphate (phosphate-SAM) and pyridine (pyridine-SAM) pointing towards the solution. To remove the molecules that did not bind to the Au substrate, tips were rinsed and stored in ethanol for at least 20 min prior to use. The quality of the functionalisation and the thickness of the SAM was checked with XPS on an Au substrate (~4x4 cm), functionalised using the same procedure as for the tips. The spectra were charge referenced by setting the $Au_{4f7/2}$ line to 84.0 eV. Figure S1 shows a clean Au substrate (middle), a pyridine-SAM (top) and a phosphate-SAM (bottom). All three surfaces contained only elements attributable to the Au substrate and functionalising molecules: C, S, O and P from 11-mercaptoundecylphosphoric acid or C, S and N from 4-(12-mercaptododecyl)pyridine, suggesting no contamination except adventitious carbon on the pure Au surface. Figure S2 shows successful formation of the Au-S bonds (bound thiols) between the S-containing head groups of the functionalising molecules and the Au-substrate. The position of the S_{2p} line in the pyridine-SAM (Figure S1a) suggests that all S bonded to Au,[4] whereas the ratio of bound to unbound thiol in the case of the phosphate-SAM is 72:28 (Figure S1b). To confirm that the bulk unbound thiol does not sit on top of the phosphate-SAM, we approximated the thickness of the organic overlayer, *d*, by taking a standard expression:[5,6]

$$d = -\lambda_{Au/SAM} \ln\left(\frac{I_{Au}}{I^0{}_{Au}}\right), \qquad (1)$$

where $\lambda_{Au/SAM}$ represents the attenuation length of $Au_{4f7/2}$ photoelectrons in the hydrocarbon overlayer

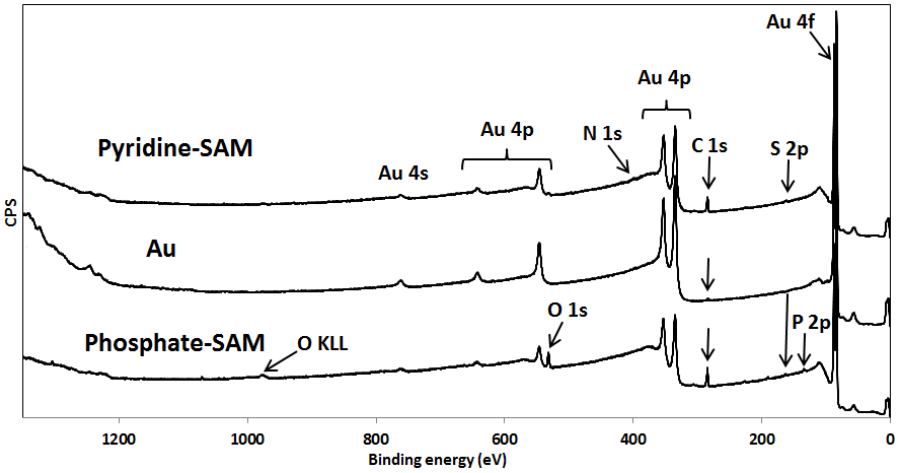

Figure S1 XPS wide spectra from pure Au (middle), Au functionalised with pyridine (top) and phosphate SAMs (bottom).

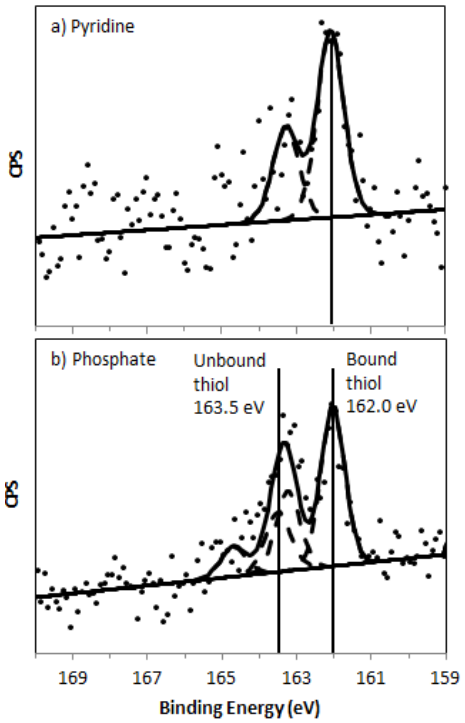

Figure S2 High resolution XPS spectra of a) 4-(12-mercaptododecyl)pyridine and b) 11-mercaptoundecylphosphoric acid on a Au substrate. a) $S_{2p1/2}$ at 162.0 eV suggests the presence of only bound thiol. b) Besides the line at 162.0 eV representing thiol bound to Au, an additional line at 163.5 eV represents unbound thiol; the ratio of unbound to bound thiol is 72:28.

(taken as 42 Å[7]), I_{Au} represents $Au_{4f7/2}$ line intensity of the SAM-covered Au substrate and I^{0}_{Au} represents the $Au_{4f7/2}$ line intensity of the clean Au substrate (separately measured under the same instrument and acquisition settings). The thickness, 19.7 Å, is close to the SAM thickness (20 Å) measured for an alkane of similar length with only a carboxylic instead of phosphoric functional group.[8] This thickness suggests

formation of a monolayer[9] so we do not expect an excess of 11-mercaptoundecylphosphoric acid to be sitting on top of the phosphate-SAM and interfering with measurements. The thickness of the pyridine-SAM was 13.4 Å, also suggesting single monolayer formation.

4. DFS measurement

The DFS measurements were made to obtain the absolute bond parameters between organic functional groups representing active adsorption sites on nucleotide and model mineral surfaces representing clay minerals. The bond parameters were then used for calculating the Gibbs free energy of binding, ΔG_{bu}.

All experiments were made in 10 mM NaCl solutions at pH=3. Stock solution of 10 mM NaCl (Sigma Aldrich) was prepared and equilibrated to pH 3 using 0.5 M HCl (Sigma Aldrich). We used an Asylum Research MFP-3D AFM. Substrates were loaded into the liquid cell and covered with NaCl stock solution. To minimise the possibility of damaging the tip, we gently approached the surface in tapping mode. The spring constant was obtained following the experiment. Seven retracting velocities, between 5 and 10,000 nms^{-1}, were chosen to probe the near equilibrium and the kinetic regimes, corresponding to loading rates between 0.7 and 120 nNs^{-1}. All measurements had an approach velocity of 100 nms^{-1}, surface dwell time of 0.5 s and trigger point of 100 pN. During the measurements, the tip made a random walk over the surface with a step distance of 10 nm. We collected at least 100 force curves per retracting velocity, resulting in at least 700 force curves per measurement.

The hematite and corundum substrates were cleaned between measurements to avoid accumulation of organic contamination and change of nonspecific, interaction forces. The mica substrate was used in a couple of subsequent measurements and the averaged forces from subsequent measurements were combined for data analysis. This is the reason for 7 data points for hematite-phosphate and corundum-phosphate plots but 14 points for mica-pyridine/phosphate plots (Figure 3). Figure S3 shows there are no significant differences in the trend of rupture forces over the course of the experiments, showing that the mineral surfaces were not accumulating contamination and the tip was not being damaged over the course of the experiment.

5. DFS data processing

Data were analysed using the method reported by Friddle et al.[10] DFS plots show the average rupture force, *f*, as a function of the logarithm of the applied loading rate. *f* is calculated as the average of all rupture forces for a given loading rate. Effective loading rates were determined from the product of the apparent retraction velocity and the spring constant of the cantilever. This approach is valid because the alkanethiol SAM's are not elastic so the whole cantilever-SAM system behaves as a stiff probe. When a sufficiently broad range of loading rates is probed, two regimes can be recognised in a *f* vs. log(loading rate) plot: a near equilibrium regime and a kinetic regime.[10,11] The near equilibrium regime covers conditions at which the loading rate is small enough for a bond to reform during the separation of two molecules while in the kinetic regime, the loading rates are too strong for the bond to reform once it is broken. In the *f* vs. log(loading rate) plots, the near equilibrium regime is recognised as plateaued values of average forces at low loading rates and a kinetic regime is recognised as values of average forces steeply increasing at higher loading rates (Figure 3a,b). Fitting the DFS data to the dependency between rupture forces and loading rates in case of formation of multiple bonds between the tip and the substrate, we obtained: i) the equilibrium rupture force at static conditions, f_{eq}, ii) the distance between the bound and the transition state, x_t, and iii) the thermal off-rate i.e. the intrinsic unbinding rate in the absence of applied force, k_{off}.

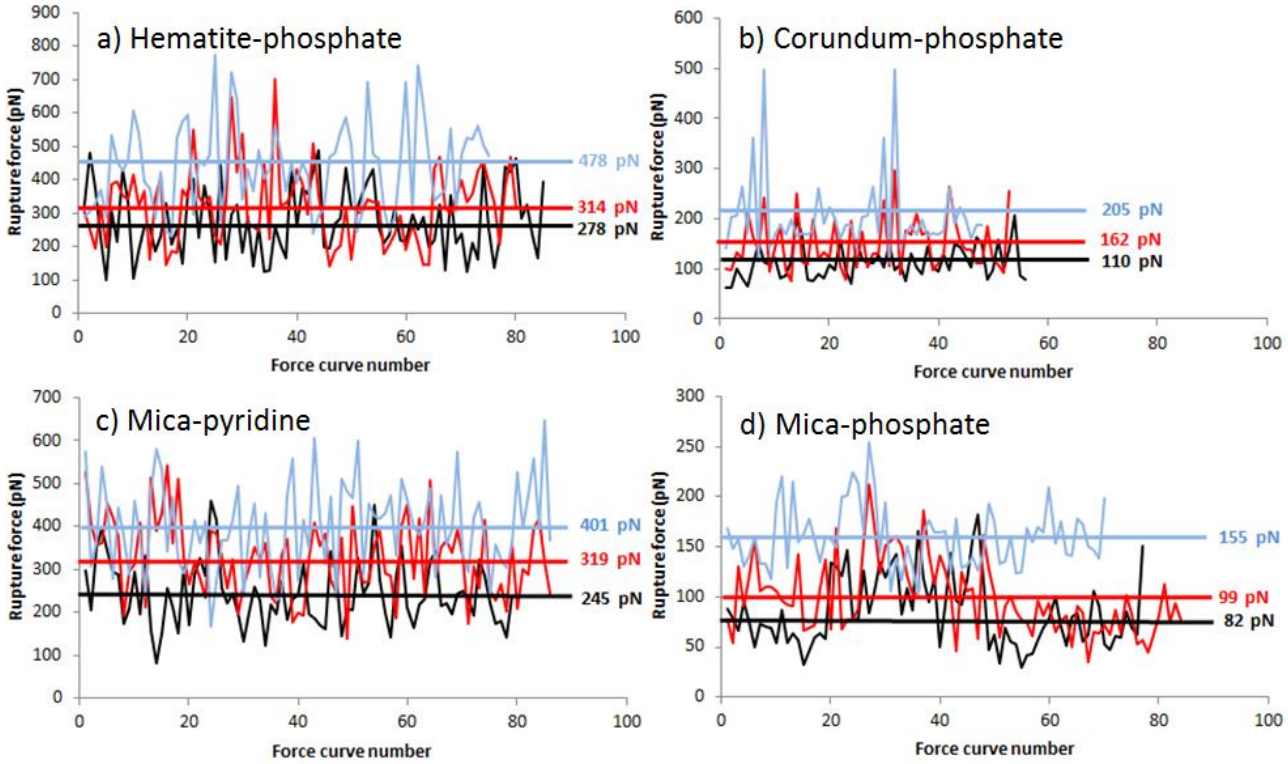

Figure S3 Plots of rupture forces of single force curves collected over the course of the experiment for lowest (black), middle (red) and highest (blue) loading rates for interactions of a) hematite-phosphate, b) corundum-phosphate, c) mica-pyridine and d) mica-phosphate. The numbers on the right are calculated average rupture forces for given loading rates. They show no systematic change in the trend of rupture forces during the experiment.

117 ΔG_{bu} can then be determined by taking Equation (8) of Friddle et al. (2012)[10]:

118 $$f_{eq} = \frac{k_B T}{x_t} W\left(e^{\left(\frac{\Delta G_{bu}}{k_B T} - 1\right)}\right), \qquad (2)$$

119 where k_B represents the Boltzmann constant, T, the absolute temperature and W, the Lambert function
120 defined as:

121 $$x = W(x) e^{W(x)} . \qquad (3)$$

122 Rearranging Equation (2):

123 $$\frac{f_{eq} x_t}{k_B T} = W\left(e^{\left(\frac{\Delta G_{bu}}{k_B T} - 1\right)}\right), \qquad (4)$$

124 and considering:

125 $$x = e^{\left(\frac{\Delta G_{bu}}{k_B T} - 1\right)}, \qquad (5)$$

126 then by combining Equations (4) and (5), we obtain:

127 $$e^{\left(\frac{\Delta G_{bu}}{k_B T} - 1\right)} = \frac{f_{eq} x_t}{k_B T} e^{\frac{f_{eq} x_t}{k_B T}}. \qquad (6)$$

128 By further developing Equation (6) we obtain:

129 $$\Delta G_{bu} = k_B T \ln \frac{f_{eq} x_t}{k_B T} + f_{eq} x_t + k_B T. \qquad (7)$$

130 We want to emphasise that the reason there is no term for the effective spring constant of the cantilever in
131 Equations (2-7) is that, when many bonds form, the ΔG_{bu} (and f_{eq}) are determined by the ensemble of bonds
132 that break and reform between the probe and the surface, and not by the spring constant, as is the case for
133 a single bond where there is only one interaction between the surface and the unbound state at the end of
134 a cantilever[10].
135 The length of alkanethiols decorating the tip is much shorter than the curvature of the tip, and we can
136 therefore expect formation of multiple bonds between the tip and the substrate.[10] The number of bonds,
137 N, in the DFS experiment influences the values for both f_{eq} and x_t. It is not possible to deduce single
138 molecule interactions from the alkanethiol SAMs because the alkanethiols are not flexible and the elastic
139 response of the linker cannot be used to discriminate single molecule force curves. However, the exact
140 knowledge of N is not necessary for comparison among different datasets as long as N remains relatively

similar throughout the experiments. To estimate the variability between our functionalised probes and to ensure that we report significant trends between our experimental systems, we tested multiple tips of the same type and functionalisation, similar radii and spring constants to estimate variability. For our analysis, we used a verified approach[12,13] where we only considered measurements that yielded values for x_t ~1 Å, which are typical of single molecule bonds[14] while much smaller values result from multiple bonds[10]. This approach allows us to compare the results between experiments. We cannot be certain, however, that these measurements are actually single molecule interactions and for that reason we are applying a multibond model[10] for the data treatment. Table S1 shows the average obtained values with uncertainty expressed as half of the range for the four experimental systems.

Table S1

	Hematite—phosphate (n=6)[a]	Corundum—phosphate (n=4)	Mica—phosphate (n=3)	Mica—pyridine (n=3)
x_t (Å)	0.4 ± 0.1[b]	1.1 ± 0.1	1.2 ± 0.1	0.7 ± 0.1
f_{eq} (pN)	255 ± 20	94 ± 9	78 ± 8	235 ± 15
ΔG_{bu} (kT)	5.4 ± 1.0	4.8 ± 0.2	3.9 ± 0.1	6.5 ± 1.0

[a] n= number of experiments that yielded values for x_t~1 Å
[b] uncertainty expressed as half of the range, i.e. (max—min)/2

The experiments shown in Figure 3 were chosen because they have a f_{eq} close to the average f_{eq}. The averaged values (Table S1) are not reported in the manuscript for two reasons:

i) we cannot know if the measurements that are being averaged represent the same number of bonds between the tip and the substrate and

ii) the values of x_t and f_{eq} for each measurement are most likely already values averaged over a few bonds, i.e. over the course of one DFS experiment. Hence, we have to assume that each force curve represents a different number of interacting bonds that is averaged once we make the fit.

With this approach, the results we report in Figure 3 are representative and we emphasise that taking the average ΔG_{bu} from Table S1 instead, would not change our discussion nor conclusions. Thus, our measurements with different tips on different substrates are internally consistent and the relative relationships between measured systems can be considered to be correct, e.g. ΔG_{bu}(mica-pyridine)/

166 ΔG_{bu}(mica-phosphate) = 1.6 ± 0.3 kT, ΔG_{bu}(mica-pyridine)/ ΔG_{bu}(hematite-phosphate) = 1.1 ± 0.2 kT and
167 ΔG_{bu}(hematite-phosphate)/ ΔG_{bu}(corundum-phosphate) = 1.1 ± 0.2 kT etc.

168 **6. The off-rates and uncertainty of the fitting parameter**

169 The large uncertainties in the k_{off} of hematite-phosphate and mica-pyridine are a consequence of too
170 few probed loading rates in the kinetic regime. How many loading rate data points there are in the near
171 equilibrium and how many in the kinetic regime depends on the range of the probed retracting velocities
172 for a given AFM tip, i.e. the spring constant of the cantilever. Using very high retracting velocities results in
173 a viscous drag exerted on the cantilever, retarding the pulling force and recording a smaller force than is
174 actually applied.[15] Because our results are only internally consistent and depend on the AFM tip used, the
175 range of loading rates we were able to probe was limited. We considered it to be more important to get
176 more points in the near equilibrium region and in the range of loading rates that define the transition
177 between the near equilibrium and the kinetic regime because those regions are more important for the
178 estimation of the f_{eq} and, x_t. Unlike k_{off}, these parameters are necessary for the calculation of the ΔG_{bu}
179 (Equation 7).

180 **7. Surface charge density difference between phosphate-SAMs and pyridine-SAM and its influence on the**
181 **measured** ΔG_{bu}

182 To ensure that the observed differences in ΔG_{bu} measurements between mica-phosphate, corundum-
183 phosphate and hematite-phosphate, and mica-pyridine are not simply because of different surface charge
184 densities between the phosphate-SAM and the pyridine-SAM, we have estimated the ionisation fraction of
185 functional groups of SAMs, f_i, by taking:

186 $$f_{i1} = \left(\frac{[HPO_4^-]}{[H_2PO_4]+[HPO_4^-]}\right) = \frac{\frac{[HPO_4^-]}{[H_2PO_4]}}{1+\frac{[HPO_4^-]}{[H_2PO_4]}}, \qquad (8)$$

187 $$f_{i2} = \left(\frac{[C_5H_5N^+]}{[C_5H_5N]+[C_5H_5N^+]}\right) = \frac{\frac{[C_5H_5N^+]}{[C_5H_5N]}}{1+\frac{[C_5H_5N^+]}{[C_5H_5N]}} \qquad (9)$$

188 where [ ] represents the activity of a species. By taking into account the dissociation constants, K_d, for
189 phosphate-SAM and pyridine-SAM at low pH, we obtain:

190 $$K_{d1} = \frac{[HPO_4^-][H^+]}{[H_2PO_4]}, \qquad (10)$$

191 $$K_{d2} = \frac{[C_5H_5N][H^+]}{[C_5H_5N^+]}. \quad (11)$$

192 Rearranged, these equations yield:

193 $$pK_{d1} = pH - log\frac{[HPO_4^-]}{[H_2PO_4]}, \quad (12)$$

194 $$pK_{d2} = pH - log\frac{[C_5H_5N]}{[C_5H_5N^+]} \quad (13)$$

195 and expressing them as ratios between charged and uncharged species we get:

196 $$\frac{[HPO_4^-]}{[H_2PO_4]} = 10^{(pH-pK_{d1})} \quad (14)$$

197 $$\frac{[C_5H_5N^+]}{[C_5H_5N]} = 10^{(pK_{d2}-pH)} \quad (15)$$

198 Inserting Equation (14) in Equation (8) and Equation (15) in Equation (9), we finally obtain:

199 $$f_{i1} = \frac{10^{(pH-pK_{d1})}}{1+10^{(pH-pK_{d1})}}, \quad (16)$$

200 $$f_{i2} = \frac{10^{(pK_{d2}-pH)}}{1+10^{(pK_{d2}-pH)}}. \quad (17)$$

201 f_i estimates the surface charge of a SAM as a function of how far pH is from the equilibrium acid
202 dissociation constant, pK_a. Taking for $pK_{d1} = pK_{a3(\text{phosphoric acid})} = 2.1$[16] and for $pK_{d2} = pK_{a(\text{pyridine})} = 5.3$[17], we find
203 from Equations (16) and (17) that, at pH = 3, $f_{i1} = 0.9$, suggesting that 90% of phosphate in the phosphate-
204 SAM carries a charge and that $f_{i2} = 1$, suggesting 100% of pyridine in the pyridine-SAM carries a charge. The
205 surface charge density of our SAMs must be solely a function of f_i, assuming that the structure of
206 alkanethiol monolayers is similar regardless of the chain terminating functional groups[18] and that,
207 consequently, the packing densities of SAMs are similar. Thus, by calculating a ratio between ionisation
208 fraction for pyridine and phosphate SAMs, $f_{i2}/f_{i1} = 1.1$, and assuming a linearity between the surface charge
209 density and ΔG_{bu}, we conclude that any difference between ΔG_{bu} of substrate-phosphates and mica-
210 pyridine, where $\Delta G_{bu(\text{mica-pyridine})}/\Delta G_{bu(\text{substrate-phosphate})} \geq 1.1$ cannot be a consequence of difference in surface
211 charge density of the SAMs. $\Delta G_{bu\ (\text{mica-pyridine})}/\Delta G_{bu(\text{mica-phosphate})} = 1.6$ and $\Delta G_{bu\ (\text{mica-pyridine})}/\Delta G_{bu(\text{corundum-phosphate})} =$
212 1.3 ratios are higher than 1.1 and the difference cannot be related to the surface charge densities of SAMs.
213 $\Delta G_{bu\ (\text{mica-pyridine})}/\Delta G_{bu(\text{mica-hematite})} = 1.1$ and this difference can result from surface charge density difference.
214 However, the hematite-phosphate and mica-pyridine ΔG_{bu} have overlapping standard deviations. Hence,
215 this discussion does not change our interpretation of the data or the conclusions.

REFERENCES:

1. D. Argyrys, A. Phan, A. Striolo and P.D. Asbhy, *J. Phys. Chem. C* 2003, **117**, 10433–10444.

2. N.A. Burnham, X. Chen, C.S. Hodges, G.A. Matei, E.J. Thoreson, C.J. Roberts, M.C. Davies and S.J.B. Tendler, *Nanotechnology* 2003, **14**, 1-6.

3. K.M.S. Juhl, N. Bovet, T. Hassenkam, K. Dideriksen, C.S. Pedersen, C.M. Jensen, D.V. Okhrimenko and S.L.S. Stipp, *Langmuir* 2014, **30**, 8741-8750.

4. D.G. Castner, K. Hinds and D.W.Grainger, *Langmuir* 1996, **12**, 5083-5086.

5. C.D. Bain and G.M. Whitesides, *J. Phys. Chem.* 1989, **93**, 1670-1673.

6. C.D. Bain and G.M. Whitesides, *J. Am. Chem. Soc.* 1989, **111**, 7164-7175.

7. P.E. Laibinis, C.D. Bain and G.M. Whitesides, *J. Phys. Chem.* 1991, **95**, 7017-7021.

8. S.D. Techane, L.J. Gamble and D.G. Castner, *J. Phys. Chem. C* 2011, **115**, 9432-9441.

9. J.C. Love, L.A. Estroff, J.K. Kriebel, R.G. Nuzzo and G.M. Whitesides, *Chem. Rev.* 2005, **115**, 1103-1169.

10. R.W. Friddle, A. Noy and J.J. De Yoreo, *Proc. Natl. Acad. Sci. U.S.A* 2012, **109**, 13573-13578.

11. A. Noy, Curr. Opin. *Chem. Biol.* 2011, **15**, 710-718.

12. Hamm, L.M., Giuffre, A.J., Han, N., Tao, J., Wang, D., De Yoreo, J.J., Dove, P.M. *PNAS* 2014, **111**, 1304-1309.

13. Newcomb, C.J., Qafoku, N.P., Grate, J.W., Bailey, V.L., De Yoreo, J.J. *Nat. Comm.* 2017, **8**, 396.

14. B.M. Pettitt and M. Karplus, *J. Chem. Phys.* 1985, **83**, 781–789.

15. E. Evans, Annu. *Rev. Biophys. Biomol. Struct.* 2001, **30**, 105–128.

16. K.J. Powell P.L. Brown, R.H. Byrne, T. Gajda, G. Hefter, S. Sjøberg and H. Wanner, *Pure Appl. Chem.* 2005, **77**, 739–800.

17. M.P. Andersson, M.H.M. Olsson and S.L.S. Stipp, *Langmuir* 2014, **30**, 6437–6445

18. R.G. Nuzzo, L. H. Dubois and D. L. Allara, *J. Am. Chem. Soc.* 1990, **112**, 558.